Environmental Science & Technology

ARTICLE

pubs.acs.org/est

Effect of pH on Aqueous Se(IV) Reduction by Pyrite

Mingliang Kang,[†,‡] Fanrong Chen,[*,†] Shijun Wu,[†] Yongqiang Yang,[†] C. Bruggeman,[§] and L. Charlet[∥]

[†]Guangzhou Institute of Geochemistry, Chinese Academy of Sciences, Guangzhou 510640, China

[‡]Graduate University of Chinese Academy of Sciences, Beijing 100049, China

[§]SCK.CEN, Research unit R&D Waste Disposal, Boeretang 200, B-2400 Mol, Belgium

[∥]Environmental Geochemistry Group, LGIT-OSUG, Grenoble University, 38041 Grenoble Cedex 9, France

Supporting Information

ABSTRACT: Interaction of aqueous Se(IV) with pyrite was investigated using persistently stirred batch reactors under O_2-free (<1 ppm) conditions at pH ranging from ~4.5 to ~6.6. Thermodynamic calculations, an increase in pH during the experiments, and spectroscopic observation indicate that the reduction of aqueous Se(IV) by pyrite is dominated by the following reaction: $FeS_2 + 3.5HSeO_3^- + 1.5H^+ = 2SO_4^{2-} + Fe^{2+} + 3.5Se(0) + 2.5H_2O$. The released Fe(II) was partitioned between the bulk solution and pyrite surface at pH ≈ 4.5 and 4.8, with the Fe^{2+} density at pyrite-solution interface about 4 orders of magnitude higher than that in the bulk solution, while iron oxyhydroxide precipitated at pH ≈ 6.6, resulting in the decrease of dissolved iron. In the Se(IV) concentration range of the experiments, aqueous Se(IV) reduction rate follows the pseudofirst order which is in the form of $\ln m_{Se(IV)} = -k't + \ln m_{Se(IV)}^0$, where k' is apparent rate constant combining the rate constant k and pyrite surface area to mass of solution ratio (A/M). And the aqueous Se(IV) reduction rate constant for a standard system (k) with 1 m^2 pyrite surface area per 1 kg solution was obtained to be 1.65×10^{-4} h^{-1}, 3.28×10^{-4} h^{-1}, and 4.76×10^{-4} h^{-1} at pH around 4.5, 4.8, and 5.1, respectively. The positive correlation between reaction rate and pH disagrees with the theories that protons are consumed when $HSeO_3^-$ is reduced to Se^0, and negative charge density on pyrite surface increases as pH increases. Thus, a ferrous iron mediated electron transfer mechanism is proposed to operate during the reduction of aqueous Se(IV) by pyrite. pH and iron concentration affect significantly on Se(IV) reaction rate and reaction product.

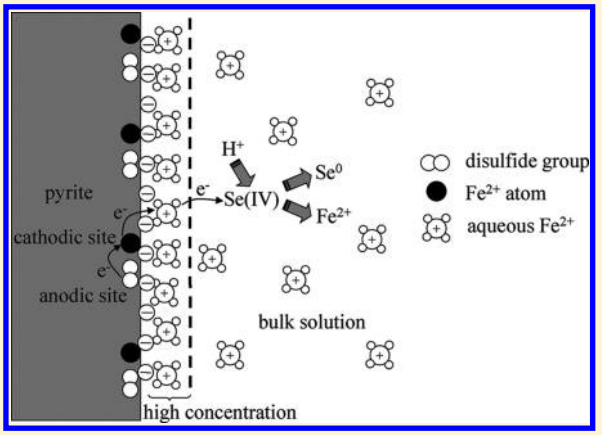

INTRODUCTION

The safe disposal of high level nuclear waste (HLW) has been a challenge worldwide, and deep geological disposal is so far the most widely accepted approach to permanently isolate the radionuclides from biosphere. Evolution scenarios of the repository suggest that over geological time scale releases of radionuclides are inevitable.[1]

The radioactive isotope ^{79}Se with a half-life of 2.95×10^5 years[2] is presently considered as the key mobile fission product for the disposal of spent fuel (SF) and high-level radioactive waste (HLW).[3] In addition, selenium is an essential micronutrient for humans and animals, and problems of both Se toxicity and deficiency occur in different parts all over the world.[4,5] Therefore, the mobility and bioavailability of Se has long been a major interest of soil and environment sciences[6−8] and an important concern for the safe disposal of HLW.[9−16]

^{79}Se is a redox-sensitive radionuclide and its solubility is largely controlled by oxidation state, depending on redox conditions. Selenite and selenate prevail as mobile aqueous oxyanions, while the oxidation states 0, -I, and -II prevail as solids with low solubility.[3,12] Pyrite is the most widely occurring of sulfide minerals in geological environment[17] and is known to buffer reducing conditions in clay formation.[18,19] Numerous studies have revealed that pyrite can reduce and immobilize redox-sensitive radionuclides (such as U, Se, Tc).[20−28] For pyrite interaction with aqueous Se(IV), previous research was concentrated on the identification of selenium species on pyrite surface.[20,25] But Se speciation on the pyrite surface should be a function of environmental parameters. Moreover, the rate and reaction mechanism of the aqueous reduction of Se(IV) by pyrite were unknown prior to this study.

MATERIALS AND METHODS

Chemicals. Pyrite samples used in this study were obtained from Jiguanshan ore mine, Tongling, Anhui, China. The natural sample was crushed, and the size fractions of 90−120 μm were selected through sieving. Magnetic separation was employed to

Received: October 4, 2010
Accepted: February 13, 2011
Revised: January 15, 2011
Published: March 08, 2011

dx.doi.org/10.1021/es1033553 | Environ. Sci. Technol. 2011, 45, 2704–2710

remove any pyrrhotite and iron oxide impurities. The pyrite crystals were ultrasonically washed using deionized water and ethanol to remove fine grains adhered to the crystals. The washed samples were soaked in hydrochloric acid to remove oxidized coating. After rinsing with deionized water followed by acetone, the pyrite sample was dried and stored in a O_2-free glovebox. Before adding to the reaction solution, crystals were further grinded using agate mortar in the glovebox. The specific surface area of the grinded pyrite was measured to be 0.11 $m^2.g^{-1}$ by the BET-N_2 method using a single point adsorption nitrogen process. The purity of the pyrite powder is higher than 99% according to XRD analysis (shown in Figure S1).

Sodium selenite was taken from Guangzhou Chemical Co., Ltd., with a purity >97%. All other chemicals used were of analytical grade. The water used was deionized (18.3 mΩ) and was boiled out before introducing to the glovebox.

Batch Experiments. Two series of batch experiments were conducted in an oxygen-depleted (<1 ppm O_2) glovebox (Mikrouna Company) flushed with highly purified nitrogen at room temperature (26 °C). Each reactor contained 1000 mL of solution and 7.5 g of pyrite. The suspension was continuously stirred by magnetic stirring apparatus. After 4 days equilibrium with deionized water, 0.58 g of NaCl solid was introduced as ion medium.

In the preliminary experiments which lasted 7 days, the solution pH were set around 4.5 and 6.6 using CH_3COONa (2.63 g)-CH_3COOH and NaH_2PO_3 (4.88 g)-Na_2HPO_3 (6.72 g) buffer solution, respectively. At the start of experiment, the reactors contained 0.28 g and 0.24 g of Na_2SeO_3, respectively. In the second series of experiments, the initial pH was at 4.5, 4.74, and 5.0 in reactors C, B, and A, respectively, and was buffered using CH_3COONa-CH_3COOH. Then, 4.2, 4.8, and 4.5 mL of 0.1 $mol \cdot L^{-1}$ Na_2SeO_3 solution were added, respectively, to reactors C, B, and A. The solution pH was monitored using a Satorious pH meter and adjusted using 0.1 M HCl and concentrated CH_3COOH.

At a given time interval, 5 mL suspension was sampled and immediately filtered in the glovebox using 0.22 μm pore diameter membrane. Both iron and Se(IV) concentrations in the filtrate were analyzed using inductively coupled plasma-optical emission spectroscopy (ICP-OES).

X-ray Absorption Spectroscopy. In order to investigate the selenium speciation on pyrite surface, 0.3 g of pyrite sample was sampled from reactor C (pH around 4.5) after 21 days reaction. XANES spectroscopic measurements were performed at the Se K-edge (12.658 keV) on the BL14W1 Beamline at Shanghai Synchrotron Radiation Facility (Shanghai, China). The sample was measured in fluorescence mode using a 7 element Ge detector. Red and gray Se(0), FeSe, $FeSe_2$, and Na_2SeO_3 were used as references and measured in transmission mode. The pyrite sample was sealed with Kapton tape in the glovebox (O_2 < 1 ppm). To avoid photoinduced redox reactions, the measurement was conducted in a chamber filled with inert N_2. For monochromator's energy calibration, reference gold foil (K-edge at 11919 eV) was chosen because of its greater inertness in comparison to Se. Data were collected at a step of 0.5 eV. Background subtraction and edge normalization were performed using Athena version 0.8.061.[29]

Geochemical Modeling Calculations. Geochemical modeling calculations were performed with PHREEQC code[30] or Geochemist's Workbench package,[31] using the latest NEA thermodynamic data for Se[32] and ANDRA thermodynamic data for iron chemicals,[33] implemented into the llnl.dat or the thermo V8.R6+.dat provided by Lawrence Livermore National Laboratories. The activity coefficient calculation is illustrated in the Supporting Information.

RESULTS

Rate Determination. The experimental data of the reactors are listed in Tables S2 and S3. Thermodynamic calculations indicate that $HSeO_3^-$ is the predominant aqueous Se(IV) species in the pH range between 2.56 and 8.12 (Figure S2). Furthermore, greater than 99% of the dissolved Se(IV) is $HSeO_3^-$ at pH around 5.0. On the other hand, probable reduction product of Se(IV) by pyrite includes Se(0), $FeSe_2$, and FeSe.

Oxidative dissolution of pyrite by dissolved oxygen and ferric iron (Fe^{3+}) has intensively been studied,[34−37] and the reactions are

$$2FeS_2 + 7O_2 + 2H_2O = 2Fe^{2+} + 4SO_4^{2-} + 4H^+ \quad (1)$$

and

$$FeS_2 + 14Fe^{3+} + 8H_2O = 15Fe^{2+} + 2SO_4^{2-} + 16H^+ \quad (2)$$

These reactions show that the oxidation process does not oxidize iron in the mineral (it remains Fe^{2+} as it is released into the solution). Therefore, the possible electrochemical reactions between pyrite and aqueous Se(IV) in the reactors are

$$FeS_2 + 3.5HSeO_3^- + 1.5H^+ = 2SO_4^{2-} + Fe^{2+} + 3.5Se(0) + 2.5H_2O$$
$$\Delta_r G^0_{298.15} = -579.82 \text{kJ/mol} \quad (3)$$

$$FeS_2 + \frac{14}{5}HSeO_3^- + \frac{2}{5}Fe^{2+} = 2SO_4^{2-} + \frac{7}{5}FeSe_2 + \frac{2}{5}H_2O + 2H^+$$
$$\Delta_r G^0_{298.15} = -383.98 \text{kJ/mol} \quad (4)$$

$$FeS_2 + \frac{7}{3}HSeO_3^- + \frac{4}{3}Fe^{2+} + H_2O = 2SO_4^{2-} + \frac{7}{3}FeSe + \frac{13}{3}H^+$$
$$\Delta_r G^0_{298.15} = -180.62 \text{kJ/mol} \quad (5)$$

Because no additional Fe^{2+} was introduced to the reactors, the aqueous Fe^{2+} at the start of the experiment results from the oxidative dissolution of the pyrite surface and/or the oxidation of pyrite by the residual oxygen during the pre-experiment equilibrium. Assuming that the quantity in moles of SO_4^{2-} is two times that of Fe^{2+} released from pyrite, the calculated equilibrium Se(IV) content in the initial solution ($t = 0$) of the experimental system should be in the range between 10^{-31} mol and 10^{-28} mol, significantly lower than the initial Se(IV) content in the reactors. Thus, reduction of Se(IV) by pyrite is expected to occur during the experiment.

For pyrite oxidation by DO and Fe^{3+}, it has been demonstrated that electron transfer from the sulfide to the oxidant, at the cathodic site, is the rate-determining step.[36,37] This is also true for the oxidation of many other sulfide minerals such as galena, sphalerite, chalcopyrite, and arsenopyrite.[38] Thus, it can be deduced that the rate of reactions 3, 4, and 5 are controlled by electron transfer from pyrite to aqueous Se(IV) species. Further, because these reactions are very far from equilibrium, there is no significant back reaction. These observations allow us to presume a simple rate law for the consumption of aqueous Se(IV)

$$-d[Se(IV)]/dt = k[Se(IV)]^m[FeS_2]^n[H^+]^p \quad (6)$$

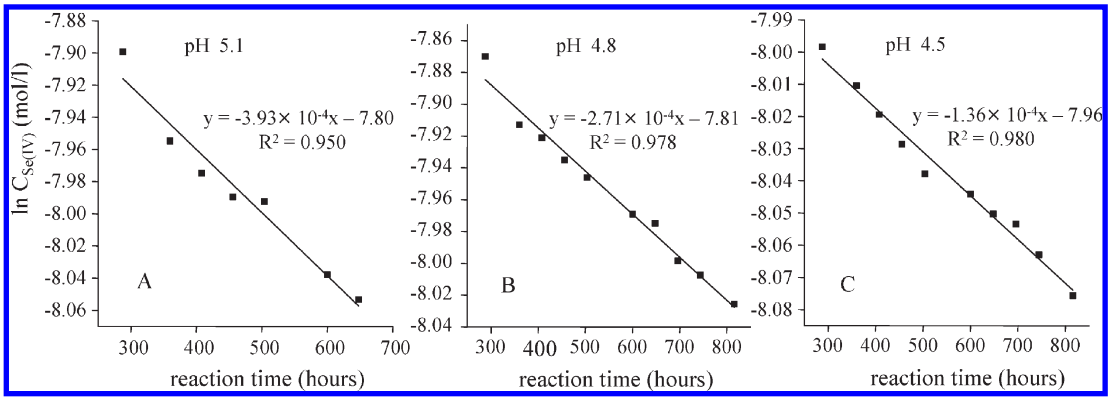

Figure 1. ln $C_{Se(IV)}$ versus reaction time t (hours) for the three series reaction pH.

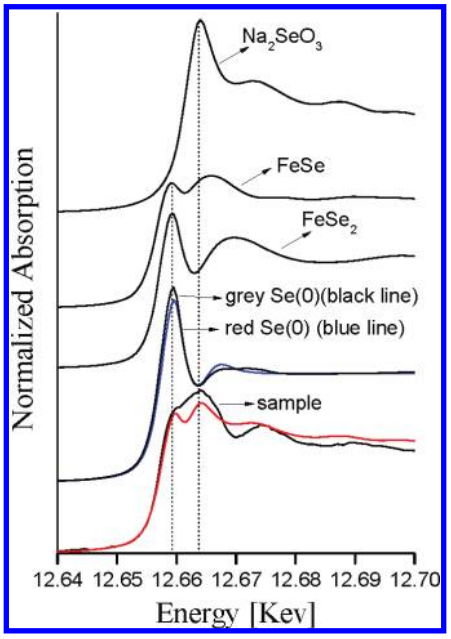

Figure 2. Se K-edge XANES spectra for sample of which pyrite interacted with Se(IV) at pH 4.5 for 21 days. Red line represents the reconstruction spectra by gray Se(0) and Na_2SeO_3 using Linear Combination Fit.

At a constant pH, the rate can be simplified to

$$-d[Se(IV)]/dt = k[Se(IV)]^m[FeS_2]^n \quad (7)$$

where k is rate constant, and $[FeS_2]$ represents the pyrite surface area to mass of solution ratio (A/M). The interaction of aqueous Se(IV) with pyrite may be described by sorption followed by a slow reduction and precipitation of a Se-solid phase or by a reductive adsorption altogether. Bruggeman et al. (2005) reported that after a short equilibration time (~7 days), interaction of pyrite with aqueous Se(IV) moved away from a simple adsorption mechanism.[16] In this study, experimental data starting from 12 days on are used for rate calculation. If the reduction rate of aqueous Se(IV) in the heterogeneous solution follows the pseudofirst order, the reduction rate is described as

$$-d[Se(IV)]/dt = k'[Se(IV)] \quad (8)$$

The integrated form of this rate law is

$$\ln m_{Se(IV)} = -k't + \ln m^0_{Se(IV)} \quad (9)$$

where k' is apparent rate constant combining the constant k and (A/M), assuming that the surface area of reacting solid per unit mass is constant because of the small extent of reaction. Figure 1 shows ln $m_{Se(IV)}$ versus time. In Figure 1, it is indicated that the reaction follows pseudofirst order in the concentration range of the experiment. The k' values at pH ≈ 4.5, 4.8, and 5.1 are obtained to be 1.36×10^{-4} h^{-1}, 2.71×10^{-4} h^{-1}, and 3.93×10^{-4} h^{-1}, respectively, by regression of the experimental data.

XANES Measurement. Figure 2 shows the Se K-edge XANES spectra of the sample from reactor C (pH 4.5) and selected Se references. Five standards were measured as reference. Linear Combination Fit (LCF) analysis indicate that a combination of gray-Se(0) and Na_2SeO_3 produces the best fit, with a consistent distribution of 54% gray-Se(0) and 46% Se(IV) in the sample, under which R-factor equal to 0.92%. XANES results demonstrate that gray-Se(0) is the reduction product when natural pyrite is reacted with aqueous Se(IV) at pH around 4.5.

DISCUSSION

Effect of pH on Reaction Rate. The aqueous Se(IV) consumption rate constant for a standard system (k) with 1 m^2 pyrite surface area per 1 kg solution can be calculated by the following equation

$$k = k'/(A/M) \quad (10)$$

For the experiments conducted in this study, A/M is 0.825 and the k values at pH = 4.5, 4.8, and 5.1 are calculated to be 1.65×10^{-4} h^{-1}, 3.28×10^{-4} h^{-1}, and 4.76×10^{-4} h^{-1}, respectively. Thus, the positive correlation between pH and log k obtained by least-squares linear regression is as follows with $R^2 = 0.97$

$$\log k = 0.77pH - 7.22 \quad (11)$$

Because $HSeO_3^-$ constitutes more than 99% of the aqueous Se(IV) and its reduction product should be elemental Se in the reactors (Figure 3), the proton consuming nature of reaction 3 suggests a negative correlation between the reaction rate and pH. Furthermore, Fornasiero et al. (1992) indicated that above pH of 2, pyrite has a negative surface charge, the density of which increases as pH increases.[39] Thus, increasing pH will inhibit the adsorption of $HSeO_3^-$. From this point of view, increasing pH will reduce the rate of pyrite-Se(IV) reaction, which also conflicts with the observation of our experiment.

On the other hand, Fe^{2+} can easily be adsorbed by a negatively charged surface and the Fe^{2+} density on pyrite surface in the reactors is several orders of magnitude higher

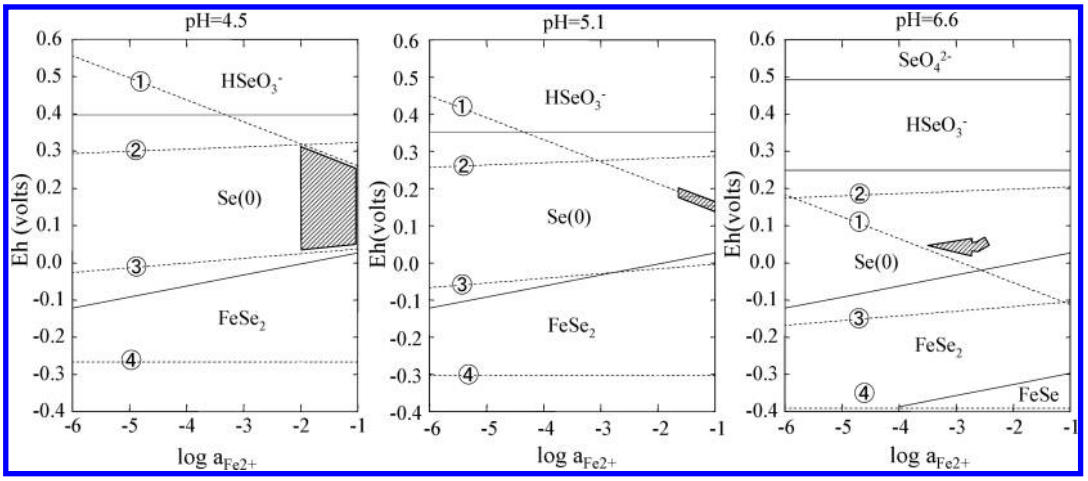

Figure 3. Eh versus log$\alpha_{Fe^{2+}}$ diagram for pyrite-Se(IV) system. For pH 4.5 and 5.1, $[Se(IV)]_{aq} = 3.3 \times 10^{-4}$ M, for pH 6.6, $[Se(IV)]_{aq} = 1$ mM. The solid lines represent the boundary between SeO_4^{2-}, $HSeO_3^-$, Se(0), $FeSe_2$, and FeSe. The dashed lines represent the following reactions: ① $Fe^{2+} + 3H_2O = Fe(OH)_3 + 3H^+ + e^-$; ② $2HSeO_3^- + Fe^{2+} + 10H^+ + 10e^- = FeSe_2 + 6H_2O$; ③ $FeS_2 + 8H_2O = Fe^{2+} + 2SO_4^{2-} + 16H^+ + 14e^-$; ④ $H_2(g) = 2H^+ + 2e^-$. The shaded areas represent the range and/or evolution of the parameters at pyrite-solution interface in the reactors.

than that in bulk solution (see below). Previous research indicated that aqueous Fe(II) sorbed on solid in heterogeneous solution could quickly reduce Se(IV) to Se(0).[14,40] We propose that the first electron transfer for pyrite-Se(IV) reaction is from Fe^{2+} that is adsorbed on pyrite surface to $HSeO_3^-$, which produces a Fe^{3+}. Subsequently, the Fe^{3+} receives an electron, at a cathodic site, from Fe^{2+} in the mineral surface. Then, an electron moves from an anodic site to the cathodic site, resulting in sulfur oxidation. The indirect electron transfer between selenite and pyrite may account for the observed relation between pH and aqueous Se(IV) reduction rate and for the much slower reaction rate as compared with pyrite oxidation rate by Fe^{3+}. Actually, the significance of dissolved ferrous iron on pyrite oxidation by DO[41] and Cr(VI)[42] has been emphasized in previous studies.

Reaction Products. Although the XANES measurement indicates that Se(0) is the Se(IV) reduction product at pH = 4.5, other Se-bearing solid phase may form as Fe^{2+} content and pH change, and a thermodynamic consideration can help to better understand the process. In the experimental system, probable Se(IV) reduction products include Se(0), $FeSe_2$, and FeSe as are indicated by reactions 3, 4, and 5, respectively. At certain pH, the stability of these solid phases is determined by Eh and Fe^{2+} activity (Figure 3). In the nonequilibrium heterogeneous system, however, the Eh at the reacting mineral (pyrite) surface cannot be represented by that of the bulk solution and has to be constrained by electrochemical reactions that would occur in the system. The following reaction of pyrite oxidation provides the lower Eh limit

$$FeS_2 + 8H_2O = Fe^{2+} + 2SO_4^{2-} + 16H^+ + 14e^- \quad (\Delta_r G^0 = 474.76\text{kJ/mol}) \qquad (12)$$

$$Eh = 0.3514 - 0.0676\text{pH} + 0.0084\log[SO_4^{2-}] + 0.0042\log[Fe^{2+}] \qquad (13)$$

Assuming that SO_4^{2-} content is two times of the iron released to the solution due to pyrite oxidation, the Eh for oxidative dissolution of pyrite can be calculated as a function of Fe^{2+} activity (Figure 3). Meanwhile, the upper Eh limit would be provided by the reduction of $HSeO_3^-$ or the precipitation of $Fe(OH)_{3(s)}$, whichever has a lower Eh or take effect. Thermodynamically, goethite is more stable than $Fe(OH)_3$, but at ambient condition and the time scale of experiment, precipitation of metastable amorphous $Fe(OH)_3$ is kinetically favorable. Therefore, we have

$$Fe^{2+} + 3H_2O = Fe(OH)_3 + 3H^+ + e^- \quad (\Delta_r G^0 = 96.48\text{kJ/mol}) \qquad (14)$$

$$Eh = 0.9998 - 0.1774\text{pH} - 0.0591\log[Fe^{2+}] \qquad (15)$$

The Eh vs log$\alpha_{Fe^{2+}}$ relation for reactions 12 and 14 are also depicted in Figure 3.

However, Fe^{2+} content at pyrite surface would be much higher than that is in the bulk solution due to ion adsorption. Parkman et al. (1999) studied the reaction of Cu^{2+} and Cd^{2+} with pyrite and mackinawite in aqueous solution and indicated that about 98% of the dissolved ions were adsorbed on the solid surface at pH around 7.[43] According to the experimental data, we estimate the specific surface area of the solid is 60 ± 30 $m^2.g^{-1}$. Assuming that the adsorbed ions are distributed within 10 Å close to the solid surface, the calculated ions density at the solid surface is about 4 orders of magnitude higher than that in the bulk solution.

According to our experimental results (Figure 4 and Table S3), the aqueous iron content increases as the reaction proceeds at pH 4.5 and 4.8. Because Se^0 is expected to be the reduction product under these pH conditions (Figure 3), reaction 3 indicates that 1 mol iron release corresponds to 3.5 mols reductive precipitation of Se^0. Figure 5 presents the correlation of the aqueous Se(IV) and iron contents during the same reaction period. Linear regressions of the plots give slopes of -3.79 at pH $\approx$ 4.5 and -5.17 at pH $\approx$ 4.8. The absolute values of the slope are larger than 3.5 that is indicated by reaction 3. Therefore, the "missing" iron of the bulk solution should be adsorbed on pyrite surface. Assuming that the adsorbed ions are distributed within 10 Å close to pyrite surface, the calculated Fe^{2+} density at pyrite surface is $\sim 2.0 \times 10^3$ and $\sim 4.8 \times 10^4$ times higher than that in the bulk solution at pH $\approx$ 4.5 and 4.8, respectively. Thus, we infer that Fe^{2+} density at pyrite surface would be in an order of five of magnitude higher than that in bulk

dx.doi.org/10.1021/es1033553 |Environ. Sci. Technol. 2011, 45, 2704–2710

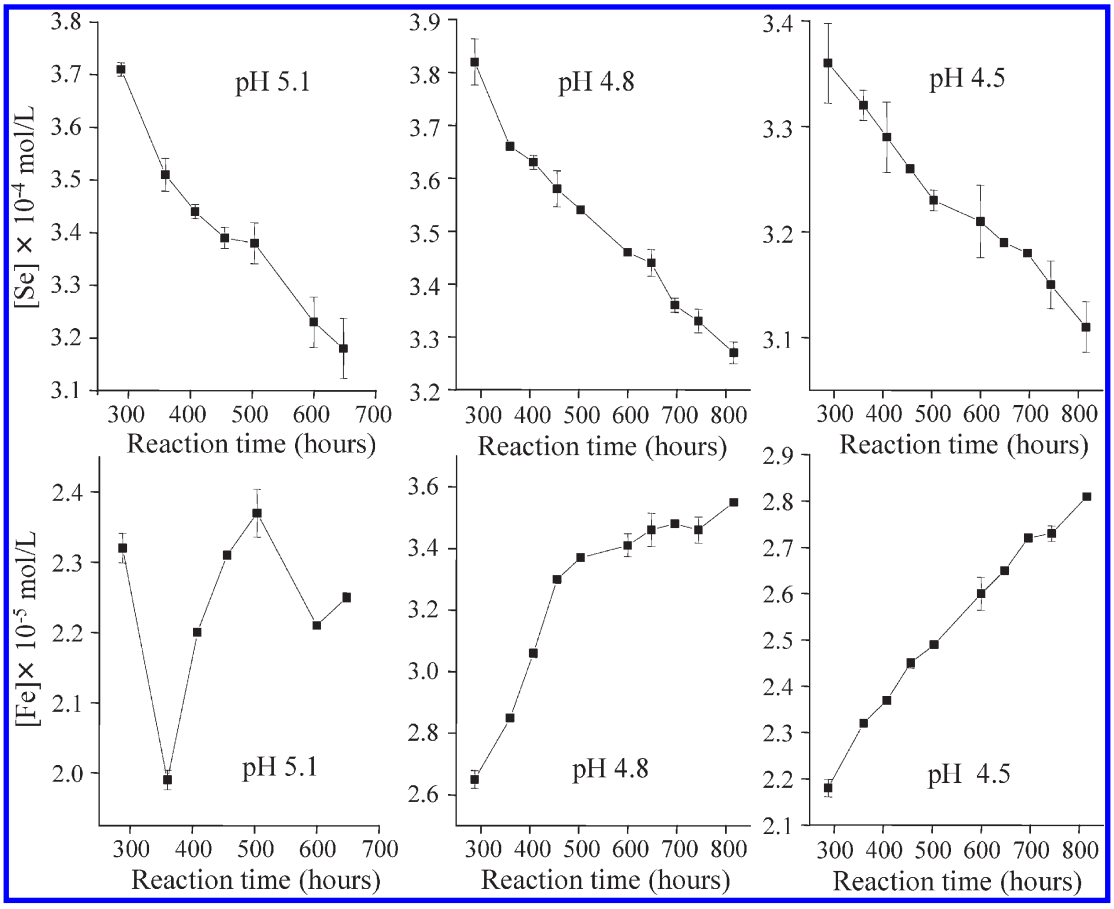

Figure 4. Variation of $[Fe]_{aq}$ and $[Se(IV)]_{aq}$ with reaction time in reactors A, B, and C. Error bar: standard deviation.

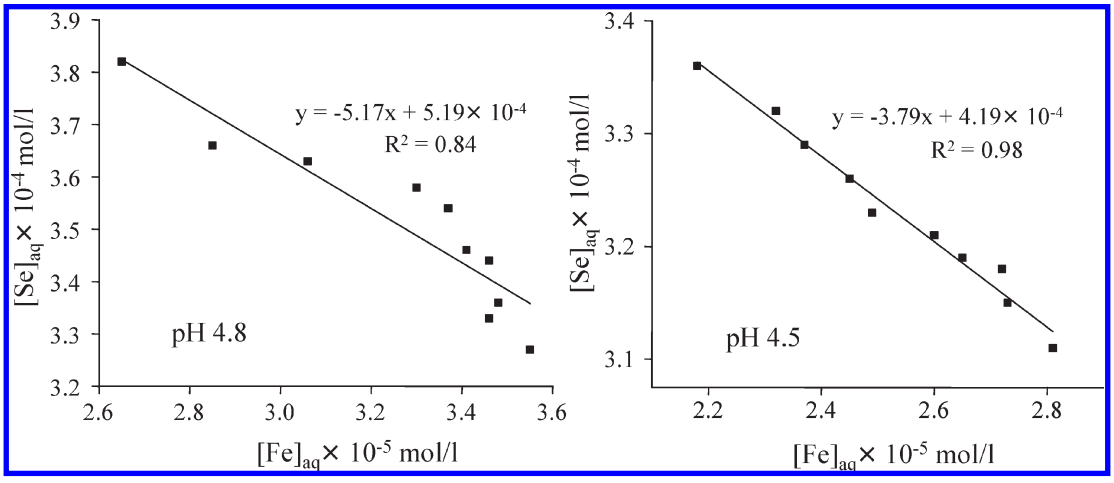

Figure 5. Correlation of aqueous Se(IV) and iron contents during the same reaction period.

solution at pH ≈ 6.6. Descostes et al. (2010) recently reported 22% of the added ^{55}Fe (2×10^{-6} mol.L^{-1}) was sorbed at pH 5.[26] As the suspension concentration is 8 g·L^{-1} and the specific area of the solid is 0.06 ± 0.004 $m^2.g^{-1}$, the surface Fe density can be calculated as 5.9×10^4 times higher than that in the bulk solution. This value is, as expected, a little higher than that is at pH ≈ 4.8 derived from our experimental data. Therefore, the estimated Fe^{2+} activity and constrained Eh range at pyrite surface at different pH are shown in Figure 3.

From Figure 3, we can see that no iron oxyhydroxide should precipitate, and the Se(IV) reduction product is Se^0 at pH = 4.5, and this is also true at pH = 4.8. Hence the relevant assumption made in the calculations above is true. At pH = 6.6, however, a initial quick decrease followed by slow decrease of dissolved iron clearly indicate that iron oxyhydroxide should be responsible for the observed removal of dissolved iron during the experiment (Table S2), and the Eh at pyrite surface would be buffered by the

following reaction

$$HSeO_3^- + 4Fe^{2+} + 9H_2O = Se(0) + 4Fe(OH)_3 + 7H^+$$
$$(\Delta_r G^0 = 84.612\text{kJ/mol}) \quad (16)$$

The oversaturate precipitation of iron oxyhydroxide demonstrates that Se(0) is the reduction product of aqueous Se(IV) at pH 6.6. Thermodynamic calculations suggest that $FeSe_2$ would form at the expense of Se(0) under near neutral and alkaline conditions, but the precipitation of iron oxyhydroxide will prohibit the formation of $FeSe_2$ at higher pH.

During the experiment at pH of 4.5, 4.8, and 5.1, concentrated CH_3COOH was added to keep pH constant, indicating that protons were consumed. This observation conflicts to the proton generating reactions 4 and 5 and indicates that Se^0 should be the reduction product of Se(IV) as is suggested by reaction 3 in these reactors. On the other hand, the relatively stable pH during the experiment at pH $\approx$ 6.6 can be explained by the simultaneous occurrence of reactions 3 and 16, which made the pH within the buffer capacity of the solution. Noticeably, some aqueous iron was removed from solution on 15th day of the experiment conducted at pH around 5.1. This iron removal coincides with a pH increase of 0.13 (Figure 4 and Table S3), indicating that precipitation of iron oxyhydroxide may occur due to such a minor pH increase in the system.

■ ASSOCIATED CONTENT

Supporting Information. Details on the XRD pattern for pyrite sample, list of the thermodynamic data used in the present study, theoretical calculation on selenium species distribution, solution analysis of the batch experiments, the principle for the activity coefficient calculation, and the thermodynamic calculation for Se(IV) reduction by pyrite. This material is available free of charge via the Internet at http://pubs.acs.org.

■ AUTHOR INFORMATION

Corresponding Author
*Phone: +86 2085290291. Fax: +86 2085290130. E-mail: frchen@gig.ac.cn.

■ ACKNOWLEDGMENT

We thank the financial support from National Natural Scientific Foundation of China (NSFC) (No. 40972213, 40573058). Also we are grateful to Shanghai Synchrotron Radiation Facility (SSRF, Shanghai, China) for performing XANES measurement. This paper was much improved by the reviewer's comments. This is contribution No. 1304 from GIGCAS.

■ REFERENCES

(1) Grambow, B. Mobile fission and activation products in nuclear waste disposal. *J. Contam. Hydrol.* **2008**, *102*, 180–186.

(2) Jiang, S.-S.; He., M.; Diao, L.-J.; Guo, J.-R.; Wu, S.-Y. Remeasurement of the half-life of ^{79}Se with the projectile X-Ray detection method. *Chin. Phys. Lett.* **2001**, *18*, 746–749.

(3) Chen, F. R.; Burns, P. C.; Ewing, R. C. Se-79: geochemical and crystallo-chemical retardation mechanisms. *J. Nucl. Mater.* **1999**, *275*, 81–94.

(4) Fordyce, F. M.; Zhang, G. D.; Green, K.; Liu, X. P. Soil, grain and water chemistry in relation to human selenium-responsive diseases in Enshi District, China. *Appl. Geochem.* **2000**, *15*, 117–132.

(5) Rayman, M. P. Food-chain selenium and human health: emphasis on intake. *Br. J. Nutr.* **2008**, *100*, 254–268.

(6) Chapman, P. M. Selenium - A potential time bomb or just another contaminant? *Hum. Ecol Risk Assess.* **1999**, *5*, 1123–1138.

(7) Siddique, T.; Zhang, Y. Q.; Okeke, B. C.; Frankenberger, W. T. Characterization of sediment bacteria involved in selenium reduction. *Bioresour. Technol.* **2006**, *97*, 1041–1049.

(8) Lin, Z. Q.; Terry, N. Selenium removal by constructed wetlands: Quantitative importance of biological volatilization in the treatment of selenium-laden agricultural drainage water. *Environ. Sci. Technol.* **2003**, *37*, 606–615.

(9) Martinez, M.; Gimenez, J.; de Pablo, J.; Rovira, M.; Duro, L. Sorption of selenium(IV) and selenium(VI) onto magnetite. *Appl. Surf. Sci.* **2006**, *252*, 3767–3773.

(10) Beauwens, T.; De Canniere, P.; Moors, H.; Wang, L.; Maes, N. Studying the migration behaviour of selenate in Boom Clay by electromigration. *Eng. Geol.* **2005**, *77*, 285–293.

(11) Scheinost, A. C.; Kirsch, R.; Banerjee, D.; Fernandez-Martinez, A.; Zaenker, H.; Funke, H.; Charlet, L. X-ray absorption and photoelectron spectroscopy investigation of selenite reduction by Fe-II-bearing minerals. *J. Contam. Hydrol.* **2008**, *102*, 228–245.

(12) Scheinost, A. C.; Charlet, L. Selenite reduction by mackinawite, magnetite and siderite: XAS characterization of nanosized redox products. *Environ. Sci. Technol.* **2008**, *42*, 1984–1989.

(13) Loyo, R. L. D.; Nikitenko, S. I.; Scheinost, A. C.; Simonoff, M. Immobilization of selenite on Fe_3O_4 and Fe/Fe_3C ultrasmall particles. *Environ. Sci. Technol.* **2008**, *42*, 2451–2456.

(14) Charlet, L.; Scheinost, A. C.; Tournassat, C.; Greneche, J. M.; Gehin, A.; Fernandez-Martinez, A.; Coudert, S.; Tisserand, D.; Brendle, J. Electron transfer at the mineral/water interface: Selenium reduction by ferrous iron sorbed on clay. *Geochim. Cosmochim. Acta* **2007**, *71*, 5731–5749.

(15) Bruggeman, C.; Maes, A.; Vancluysen, J. The interaction of dissolved Boom Clay and Gorleben humic substances with selenium oxyanions (selenite and selenate). *Appl. Geochem.* **2007**, *22*, 1371–1379.

(16) Bruggeman, C.; Maes, A.; Vancluysen, J.; Vandenmussele, P. Selenite reduction in Boom clay: Effect of FeS_2, clay minerals and dissolved organic matter. *Environ. Pollut.* **2005**, *137*, 209–221.

(17) Vaughan, D. J.; Lennie, A. R. The iron sulfide minerals-Their chemistry and role in nature. *Sci. Prog.* **1991**, *75*, 371–388.

(18) Beaucaire, C.; Pitsch, H.; Toulhoat, P.; Motellier, S.; Louvat, D. Regional fluid characterisation and modelling of water-rock equilibria in the Boom clay Formation and in the Rupelian aquifer at Mol, Belgium. *Appl. Geochem.* **2000**, *15*, 667–686.

(19) Gaucher, E. C.; Blanc, P.; Bardot, F.; Braibant, G.; Buschaert, S.; Crouzet, C.; Gautier, A.; Girard, J. P.; Jacquot, E.; Lassin, A.; Negrel, G.; Tournassat, C.; Vinsot, A.; Altmann, S. Modelling the porewater chemistry of the Callovian-Oxfordian formation at a regional scale. *C. R. Geosci.* **2006**, *338*, 917–930.

(20) Naveau, A.; Monteil-Rivera, F.; Guillon, E.; Dumonceau, J. Interactions of aqueous selenium(-II) and (IV) with metallic sulfide surfaces. *Environ. Sci. Technol.* **2007**, *41*, 5376–5382.

(21) Liu, X.; Fattahi, M.; Montavon, G.; Grambow, B. Selenide retention onto pyrite under reducing conditions. *Radiochim. Acta* **2008**, *96*, 473–479.

(22) Aubriet, H.; Humbert, B.; Perdicakis, M. Interaction of U(VI) with pyrite, galena and their mixtures: a theoretical and multitechnique approach. *Radiochim. Acta* **2006**, *94*, 657–663.

(23) Eglizaud, N.; Miserque, F.; Simoni, E.; Schlegel, M.; Descostes, M. Uranium(VI) interaction with pyrite (FeS_2): Chemical and spectroscopic studies. *Radiochim. Acta* **2006**, *94*, 651–656.

(24) Bruggeman, C.; Vancluysen, J.; Maes, A. New selenium solution speciation method by ion chromatography plus gamma counting and its application to FeS_2-controlled reducing conditions. *Radiochim. Acta* **2002**, *90*, 629–635.

(25) Breynaert, E.; Bruggeman, C.; Maes, A. XANES-EXAFS analysis of se solid-phase reaction products formed upon contacting Se(IV) with FeS_2 and FeS. *Environ. Sci. Technol.* **2008**, *42*, 3595–3601.

(26) Descostes, M.; Schlegel, M. L.; Eglizaud, N.; Descamps, F.; Miserque, F.; Simoni, E. Uptake of uranium and trace elements in pyrite (FeS_2) suspensions. *Geochim. Cosmochim. Acta* **2010**, *74*, 1551–1562.

(27) Bruggeman, C.; Maes, N. Uptake of uranium(VI) by pyrite under Boom Clay conditions: Influence of dissolved organic carbon. *Environ. Sci. Technol.* **2010**, *44*, 4210–4216.

(28) Scott, T. B.; Tort, O. R.; Allen, G. C. Aqueous uptake of uranium onto pyrite surfaces; reactivity of fresh versus weathered material. *Geochim. Cosmochim. Acta* **2007**, *71*, 5044–5053.

(29) Ravel, B.; Newville, M. ATHENA, ARTEMIS, HEPHAESTUS: Data analysis for X-ray absorption spectroscopy using ifeffit. *J. Synchrotron Radiat.* **2005**, *12*, 537–541.

(30) Parkhurst, D. L.; Appelo, C. A. J. *User's guide to PHREEQC (Version 2)-A computer program for speciation, batch-reaction, one-dimensional transport, and inverse geochemical calculations*; Water-Resources Investigations Report 99-4259; U.S. Geological Survey, U.S. Department of the Interior: Denver, CO, 1999.

(31) Bethke, C. M.; Yeakel, S. *The Geochemist's Workbench released 7.0: GWB Essentials Guide*; Hydrogeology Program, University of Illinois: **2008**.

(32) Olin, A.; Nolang, B.; Osadchii, E. G.; Ohman, L.-O.; Rosen, E. *Chemical Thermodynamics 7: Chemical Thermodynamics of Selenium*; OECD Nuclear Agency/Elsevier: Amsterdam, 2005.

(33) Chivot, J. *Thermodynamique des produits de corrosion*. Sciences et Techniques Series, ANDRA: 2004.

(34) Lowson, R. T. Aqueous oxidation of pyrite by molecular-oxygen. *Chem. Rev.* **1982**, *82*, 461–497.

(35) Hiskey, J. B.; Schlitt, W. J.; Jackson, J. S. Aqueous oxidation of pyrite. *In Situ* **1982**, *6*, 59–59.

(36) Williamson, M. A.; Rimstidt, J. D. The kinetics and electrochemical rate-determining step of aqueous pyrite oxidation. *Geochim. Cosmochim. Acta* **1994**, *58*, 5443–5454.

(37) Rimstidt, J. D.; Vaughan, D. J. Pyrite oxidation: A state-of-the-art assessment of the reaction mechanism. *Geochim. Cosmochim. Acta* **2003**, *67*, 873–880.

(38) Rimstidt, J. D.; Chermak, J. A.; Gagen, P. M. Rates of Reaction of Galena, Sphalerite, Chalcopyrite, and Arsenopyrite with Fe(III) in Acidic Solutions. In *Environmental Geochemistry of Sulfide Oxidation*; Alpers, C. N., Blowes, D. W., Eds.; ACS Symposium Series, **1993**; Vol. *550*, pp 2-13.

(39) Fornasiero, D.; Eijt, V.; Ralston, J. An electrokinetic study of pyrite oxidation. *Colloids Surf.* **1992**, *62*, 63–73.

(40) Chakrabrty, S.; Bardelli, F.; Charlet, L. Reactivities of Fe(II) on Calcite: Selenium reduction. *Environ. Sci. Technol.* **2010**, *44*, 1288–1294.

(41) Moses, C. O.; Herman, J. S. Pyrite oxidation at circumneutral pH. *Geochim. Cosmochim. Acta* **1991**, *55*, 471–482.

(42) Lin, Y. T.; Huang, C. P. Reduction of chromium(VI) by pyrite in dilute aqueous solutions. *Sep. Purif. Technol.* **2008**, *63*, 191–199.

(43) Parkman, R. H.; Charnock, J. M.; Bryan, N. D.; Livens, F. R.; Vaughan, D. J. Reactions of copper and cadmium ions in aqueous solution with goethite, lepidocrocite, mackinawite, and pyrite. *Am. Mineral.* **1999**, *84*, 407–419.